

# $^{18}\text{O}$ -tracer diffusion along nanoscaled $\text{Sc}_2\text{O}_3$ /yttria stabilized zirconia (YSZ) multilayers: on the influence of strain

Halit Aydin<sup>1</sup>, Carsten Korte<sup>2</sup> and Jürgen Janek<sup>1</sup>

<sup>1</sup> Physikalisch-Chemisches Institut, Justus-Liebig Universität Giessen, D-35390 Giessen, Germany

<sup>2</sup> Institut für Energie und Klimaforschung (IEK-3: Brennstoffzellen), Forschungszentrum Jülich, D-52428 Jülich, Germany

E-mail: [c.korte@fz-juelich.de](mailto:c.korte@fz-juelich.de)

Received 17 December 2012

Accepted for publication 9 May 2013

Published 6 June 2013

Online at [stacks.iop.org/STAM/14/035007](http://stacks.iop.org/STAM/14/035007)

## Abstract

The oxygen tracer diffusion coefficient describing transport along nano-/microscaled YSZ/ $\text{Sc}_2\text{O}_3$  multilayers as a function of the thickness of the ion-conducting YSZ layers has been measured by isotope exchange depth profiling (IEDP), using secondary ion mass spectrometry (SIMS). The multilayer samples were prepared by pulsed laser deposition (PLD) on (0001)  $\text{Al}_2\text{O}_3$  single crystalline substrates. The values for the oxygen tracer diffusion coefficient were analyzed as a combination of contributions from bulk and interface contributions and compared with results from YSZ/ $\text{Y}_2\text{O}_3$ -multilayers with similar microstructure. Using the Nernst–Einstein equation as the relation between diffusivity and electrical conductivity we find very good agreement between conductivity and diffusion data, and we exclude substantial electronic conductivity in the multilayers. The effect of hetero-interface transport can be well explained by a simple interface strain model. As the multilayer samples consist of columnar film crystallites with a defined interface structure and texture, we also discuss the influence of this particular microstructure on the interfacial strain.


Keywords: interface diffusion, ionic conductivity, strain, misfit dislocation, zirconia, nano-ionics

## 1. Introduction

The influence of interfaces on ionic transport has been one of the key issues in solid state ionics for many years. Numerous studies on the influence of structural disorder along interfaces [1–4]—leading to different charge carrier mobilities—and on the existence of space charge regions with modified charge carrier concentrations have been reported [5, 6]. Whereas poly- and nanocrystalline bulk samples were studied at the beginning, the understanding of ionic transport in nanostructured thin films is of more recent interest—driven by papers on single solid electrolyte thin films by Kosacki

*et al* [7–9] on the one hand and by papers on solid electrolyte superlattice of multilayers by Maier *et al* [10, 11] on the other. We know today that the early results for single thin films are probably spoiled by substrate short-circuits [12] and that it is difficult to assign conductivity effects unequivocally to space charge effects [28, 29]. Therefore, the experimental and theoretical study of geometrically, microstructurally and chemically well defined thin films remains a challenging research topic.

Within the last few years, coherency strain originating from heterophase boundaries in solid electrolytes, and its influence on the ionic conductivity in the strained lattice regions, has become a new subject of interest [13–17]. One reason for this interest resulted from a paper by Garcia-Bariocanal *et al* [18] in which the authors claim an increase of the ionic conductivity of up to eight orders of

 Content from this work may be used under the terms of the Creative Commons Attribution-NonCommercial-ShareAlike 3.0 licence. Any further distribution of this work must maintain attribution to the author(s) and the title of the work, journal citation and DOI.

magnitude in ultra-thin and strained yttria-stabilized zirconia films. Meanwhile, there is growing evidence that this alleged conductivity increase is rather due to electronic effects than to an increased ionic mobility [12, 19, 20]. A second reason appears to be our previous systematic work on the influence of strain on ionic conductivity in nano-scaled YSZ/RE<sub>2</sub>O<sub>3</sub> (rare earth oxides) heterophase multilayers [21, 22].

Meanwhile more experimental and theoretical studies on strain effects in ionic conductivity are being published. However, the results are often contradictory [19, 21–29], and further experimental work is required to achieve better insight.

Considering conductivity effects caused by interface from a general point of view, there exist basically three approaches to explain improved transport along interfaces: (i) models based on space charge effects [5, 6], (ii) models considering elastic strain effects [26, 28, 30, 31] or (iii) structurally disordered interface regions or misfit dislocation networks [15–18, 36]. Space charge effects can be safely neglected for systems with high concentrations of mobile charge carriers (like in YSZ), and therefore these will not be taken into account in the following [28, 29]. We instead concentrate on coherent and semi-coherent systems with well-defined lattice misfit and correspondingly, well-defined disorder at the hetero-interfaces.

One of the major problems in the quantitative interpretation of transport studies on heterophase multilayers with defined lattice misfit and coherency strain is the unknown strain release by the formation of non-equilibrium effects. In fact, we need wide areas of thin films for the measurement of lateral transport properties with macroscopic electrodes, i.e. we need typically films of several mm in width and length, but less than a  $\mu\text{m}$  in thickness. Local coherency strain will be partially released by the formation of dislocation networks and grain boundaries. Thus, thin films with slight misfit to the substrate are often nanocrystalline, and in the present case of zirconia-based solid electrolytes, the films grow columnar and thus contain a high concentration of grain boundaries. This issue is addressed by Santiso and co-workers [32] in trying to reproduce the results of Garcia-Bariocanal *et al* [18].

In [33, 34] it could be proven that poly- or nanocrystalline YSZ shows lower ionic conductivities than single crystals. This was explained by the ‘blocking effect’ for charge transfer across grain boundaries [34] due to space charge zones. Necessarily, the width of space charge zones is very small for YSZ with a high mobile charge carrier concentration, which also implies that transport along grain boundaries will not influence the transport in polycrystalline material to a serious extent. Nevertheless, enhanced ionic conductivities for YSZ thin films or multilayers were reported, assuming that interfacial misfit dislocations (fast pathways for mobile charge carriers) or strain are the reason for this [18, 26, 29].

In essence, in studying transport it is important to know the microstructure of the studied thin films in detail, in order to account properly for the contribution of strain and dislocations or grain boundaries. Thus, it is also of utmost importance to automatically generate smooth heterophase boundaries to enable a strained transition between phase 1 and phase 2 at all (cf studies of CeO<sub>2</sub>/YSZ interfaces [45] with

less well-defined microstructure and probably more or less completely relaxed strain). However, even if the system shows perfectly smooth heterophase interfaces with a negligible concentration of misfit dislocations, the quantitative effect of strain on the ionic transport properties is difficult to evaluate, because of the high concentration of the homophase grain boundaries. As mentioned, these homophase grain boundaries arise during the ablation process (PLD) and decrease the apparent bulk conductivity of the YSZ films. In summary, this means that the true effect of strain at heterophase boundaries on the ionic transport properties is superposed by homophase grain boundaries.

This problem can be reduced by comparing the ionic conductivity of strained multilayer systems with an unstrained thicker YSZ film of similar microstructure, as shown in the present paper. The single YSZ film has a comparable concentration of homophase boundaries like the strained YSZ-multilayer systems. We can use these single films as an internal standard and the effect of coherency strain at heterophase boundaries on the ionic transport properties can be separated [26, 28, 35].

One major problem in the unequivocal interpretation of conductivity effects is the question of additional electronic conductivity in the nanostructured films or substrates [19, 20]. In our previous studies (Korte *et al* [26], Peters *et al* [29] and Schichtel *et al* [28]) we investigated the effect of strain on the ionic transport properties of YSZ/RE<sub>2</sub>O<sub>3</sub> multilayer systems with impedance measurements. However, even if the grain boundary effect could be eliminated by comparison with single films, ac- and simple dc conductivity measurements always provide information on the total electron conductivity—including both ionic and electronic contributions. The risk of an increased electronic conductivity was reduced by annealing under oxidizing conditions, but we decided to perform additional oxygen tracer diffusion experiments to obtain definite information on the ionic transport.

In contrast to conductivity measurements, <sup>18</sup>O tracer diffusion experiments are not influenced by additional electronic conduction. Thus, in a recent study [35] we have already investigated the oxygen ion transport in YSZ/Y<sub>2</sub>O<sub>3</sub> multilayers as a function of the YSZ layer thickness to gain information on the ionic transport processes along the tensile strained YSZ film. We found that the mean diffusion coefficient was enhanced by a factor of about 2.5 when the thickness of the individual YSZ layer was decreased to approximately 12 nm.

In the following, we describe the experimental study of oxygen tracer diffusion in YSZ/Sc<sub>2</sub>O<sub>3</sub> multilayers. In these multilayers, YSZ is compressively strained by the insulating Sc<sub>2</sub>O<sub>3</sub> films, and the ionic conductivity is lowered—as reported by Schichtel *et al* [26, 28]. Here, we studied similar multilayer samples and compare the oxygen diffusion data with the ionic conductivity data. As a main result we obtained reliable information on possible additional (interfacial) electronic conduction in the multilayers. The diffusion data are interpreted by a simple analytical model based on interfacial strain due to lattice mismatch [21, 22].

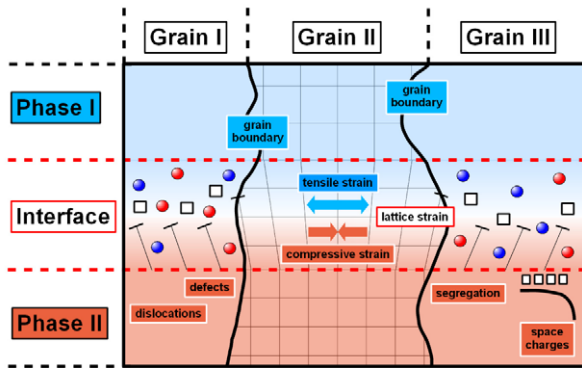


**Figure 1.** Schematic of an interfacial region between two phases consisting of three individual grains.

## 2. Formal considerations

Ionic transport processes along interfaces of crystalline solids are microscopically not as well understood as in the bulk phase. At a surface, a grain or phase boundary we find a (transition) region which is different compared to the bulk with regard to local composition and structure (see figure 1). Currently, these differences are mostly described by the effect of structural disorder and interfacial strain which are briefly introduced below.

### 2.1. Effects on interface transport due to structural disorder

A formal approach for the description of the influence of mismatch induced (coherent) elastic strain  $\varepsilon_0$  along a two-phase boundary has been primarily developed by Korte *et al* and is presented in detail in former publications [21, 22]. Here we will only summarize the major assumptions and results of this approach. In essence, the misfit-strain model is based on the assumption that misfit strain leads either (a) to local lattice distortions which change the jump frequencies of the mobile charge carriers, or (b) to severe structural rearrangements which lead to the formation of dislocation networks. Case (a) will usually be observed for small lattice misfits, and case (b) will be observed for larger misfits [37]. In practice the situation is much more complex as the geometry of the two-phase system forms an important boundary condition for the release of mechanical strain.

The microstructure of phase boundaries depends on the lattice symmetries, lattice spacings and the mutual orientation of the two adjacent lattices. In case of thin films with large extended phase boundaries between the crystallites strain release by shear is not possible. The crystallites will be completely strained, as depicted in figure 2(b). A coherent phase boundary is restricted only to crystallites with a lattice mismatch smaller than 1% [21, 22].

In the case of thin films consisting of columnar crystallites, where the diameter of the columns is large compared to their height, coherent interfaces with a negligible density of misfit dislocations can also be formed for higher mismatches. Strain release by shear is possible, locating the strain in regions close to the phase boundaries, as depicted in figure 2 (c). For the description of YSZ/insulator multilayers

we focus on strain effects in coherent heterophase boundaries between crystallites in columnar multilayers.

Due to the pressure dependence of the free activation enthalpy for an ionic jump process, also a strain dependence of ionic transport has to be expected. For the sake of simplicity we will treat the influence of strain fields with a gradient of isotropic pressure. The pressure in the strained interface region depends on Young's modulus  $Y$  and Poisson's ratio  $\nu$  of the ionic conductor and the interfacial strain  $\varepsilon_0$  due to the misfit [22]. This leads to an expression for the ratio between the ionic diffusion coefficient  $D_{\text{int}}$  close to the interface and the (unchanged) bulk value  $D_{\text{vol}}$ :

$$\ln \frac{D_{\text{int}}}{D_{\text{tot}}} = \frac{2}{3} \frac{\Delta V^{\text{m}} (V_{\text{O}}^{\bullet\bullet})}{RT} \frac{Y}{1-\nu} \varepsilon_0. \quad (1)$$

In case of YSZ,  $\Delta V^{\text{m}} (V_{\text{O}}^{\bullet\bullet})$  is the activation volume for single jumps of the oxygen vacancies (i.e. the jump of an oxygen into a vacancy). In equation (1) any anisotropy due to the crystalline structure is neglected for the reason of simplicity. For atom jumps by a vacancy mechanism the activation volume is always positive. Thus, in case of tensile interface strain ( $\varepsilon_0 > 0$ ) along the jump path, ionic transport will be enhanced and in the case of compressive interface strain ( $\varepsilon_0 < 0$ ) it will be decreased.

In this description the influence of dislocations formed along the columnar (homophase) grain boundaries is formally neglected. It may well be that these additional dislocations also increase the conductivity of the strained electrolyte film. However, as they are also caused indirectly by the interfacial misfit strain, they can be considered as an intrinsic element of the misfit-strain model.

### 2.2. Diffusion in multilayer systems

Ionic transport in a composite (layered) system parallel to the phase boundaries is composed of simultaneous boundary transport and bulk transport. Thus, in the case of a multilayer, consisting of an ionic conductor and an insulator, the values of the interface diffusion coefficient  $D_{\text{int}}$  and of the bulk diffusion coefficient  $D_{\text{vol}}$  in the ionic conducting phase determine the mean (apparent) diffusion coefficient  $D_{\text{tot}}$  as an average property of the strained conducting layer [26]. In our case,  $D_{\text{int}} \approx D_{\text{vol}}$ , resulting in type A kinetics and  $D_{\text{tot}}$  can be described by [57]

$$\frac{D_{\text{tot}}}{D_{\text{vol}}} = 1 + \left( \frac{D_{\text{int}}}{D_{\text{vol}}} - 1 \right) \frac{2\delta}{d}, \quad (2)$$

$$f = \frac{A_{\text{int}}}{A_{\text{tot}}} = \frac{2n\delta b}{ndb} = \frac{2\delta}{d}, \quad (3)$$

where  $\delta$  is the thickness of the strained interface region in the ionic conducting layers.  $A_{\text{tot}}$  is the total cross section of all  $n$  ionic conducting layers with the individual thickness  $d$  and the width  $b$ . The cross section of the strained interface regions with a modified diffusivity is denoted  $A_{\text{int}}$ .

Thus,  $f$  describes the ratio between the cross sections of the interface region and the ion-conducting film. The mean

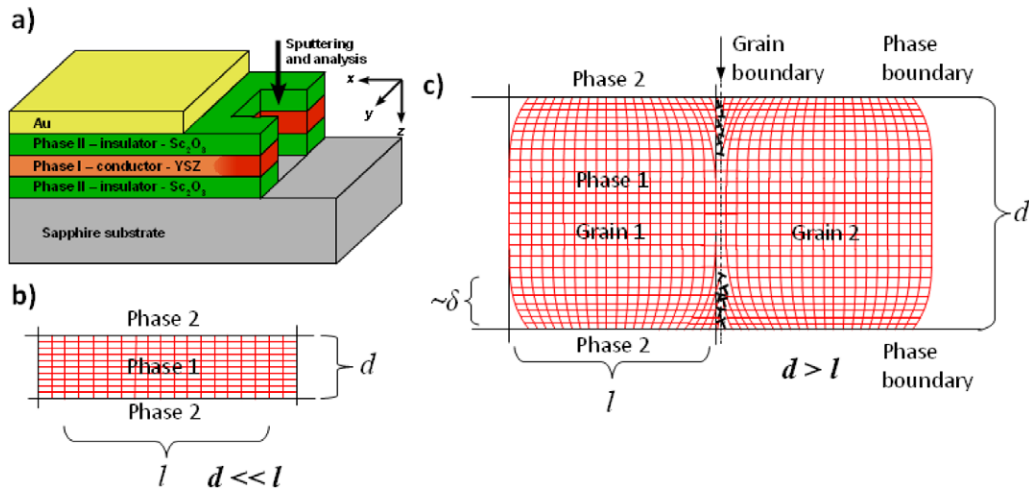


**Figure 2.** Elastic deformation of a crystallite in a multilayer thin film consisting of a phase 1 and 2. Case (a) describes the individual phases. Case (b) describes crystallites, where the height (film thickness)  $d$  is small compared to the diameter  $l$  of a grain. Case (c) describes a crystallite where the grain diameter  $l$  is small compared to its height  $d$ .

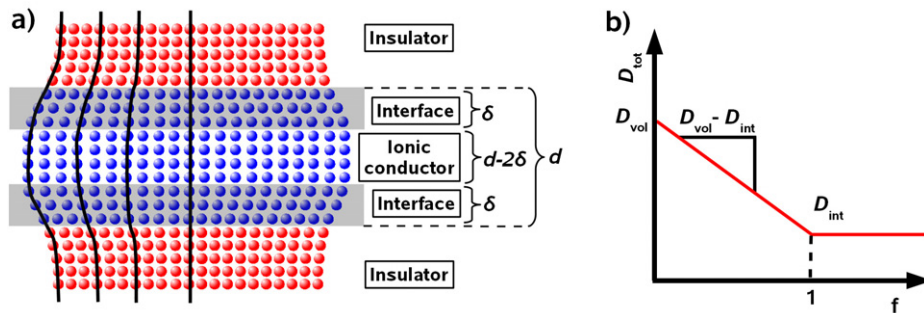


**Figure 3.** Composition of the mean diffusion coefficient  $D_{tot}$ . Case (a) shows a compressive strained individual grain between two phases and case (b) describes the dependence of  $D_{tot}$  from  $f$ .

diffusion coefficient  $D_{tot}$  is linearly dependent on the factor  $2\delta/d$ , i.e. to the factor  $f$  (see figure 3 (b)). We have to take into account that equation (3) is only valid when the layer thickness  $d$  is higher than the total thickness  $2\delta$  of the strained interfacial regions (for a better impression, see figure 3 (a)).

### 2.3. $^{18}O$ tracer diffusion experiments with multilayers

Simple electrical conductivity measurements of solid electrolytes usually provide information about the total electric conductivity. As long as we know from additional measurements that the ionic transference number is close to 1, we can safely consider the total conductivity as equal to the ionic conductivity. This assumption fails for nanostructured materials, as here the ionic conductivity may be lower due to interfacial barriers [34] and as the electronic conductivity may be higher for several reasons [56]. In principle, careful measurements of the partial conductivities with suitable electrodes are required to separate ionic and electronic contributions to the electrical conductivity. Alternatively, the ionic transport can be studied with diffusion experiments (e.g.,  $^{18}O$  tracer diffusion in YSZ), as already shown in a previous paper [35]. When the charge carrier concentration in

the solid electrolyte is known, the partial ionic conductivity can then be calculated by the Nernst–Einstein equation.

Many results for tracer diffusion coefficients of  $^{18}O$  in poly- and single-crystalline YSZ can be found in the literature [27, 34, 38–43], but to the best of our knowledge there has been no systematic study on the diffusion along interfaces in nanoscaled solid electrolyte multilayers reported to date. In the following two experimental studies comparable approaches have been reported, but without the variation of the film thickness.

In 2010, Cavallaro *et al* [20] reported one  $^{18}O$  tracer diffusion experiment on a YSZ/STO multilayer system. The result of this experiment was not useful because the sample was not gastight and diffusion of  $^{18}O$  perpendicular to the multilayer system could not be avoided. Thus, only a distorted diffusion profile along the individual YSZ layers was observed.

Recently, Pergolesi *et al* [44] studied  $^{18}O$  diffusion along  $CeO_2$ /YSZ films. Here, the microstructure of the films—as visible in transmission electron microscopy (TEM) images—did probably not lead to appreciable strain because of the rough hetero-interfaces and the high concentration of misfit dislocations. Thus, these multilayer systems appear not

to be suitable for the study of the influence of interfacial strain on ionic transport properties.

In order to investigate the tracer diffusion coefficient of YSZ in dependence of the hetero-interface density by  $^{18}\text{O}$  tracer diffusion experiments, multilayer samples with sufficiently well-defined interfaces are needed. In this study, we use multilayer samples of the type YSZ/ $\text{Sc}_2\text{O}_3$ , comparable to multilayers previously reported by us for YSZ/ $\text{Y}_2\text{O}_3$ . The tracer diffusion coefficients were determined by a SIMS-based technique (described in detail in the experimental section).

#### 2.4. YSZ/ $\text{RE}_2\text{O}_3$ model systems for the investigation of interface transport with variable interface strain

The influence of interface structure/strain on ionic transport properties is still not well understood. Korte and co-workers [22] proposed a theoretical model which is based on misfit strain, dislocations and the resulting modified mobilities along hetero-interfaces. The results of this model could successfully be verified through a specific choice of defined multilayer systems consisting of YSZ-layers as ionic conductors and rare earth oxides as insulators. The chosen  $\text{RE}_2\text{O}_3$  insulators crystallize in the bixbyite structure which is similar to the cubic  $\text{CaF}_2$  structure when doubling the lattice parameter  $a$  and simultaneously removing 16  $\text{O}^{2-}$ -ions. As a consequence of choosing different insulating  $\text{RE}_2\text{O}_3$  layers, the lattice mismatch to YSZ can be systematically varied which leads to different elastic strain, as depicted in figure 3(a), and different concentrations of non-equilibrium defects like misfit dislocations. Furthermore these model multilayer systems enable one to clearly identify the effect of interfaces on the ionic conductivity by increasing the density of interfaces (thinner individual YSZ layers and constant volume). When the density of interfaces gets higher, the influence on the ionic conductivity gets larger.

We note that this model only applies strictly when the thermal expansion coefficients of YSZ and  $\text{Sc}_2\text{O}_3$  are similar. However, the thermal expansion coefficients of YSZ and  $\text{Sc}_2\text{O}_3$  are both in the range of  $10^{-5} \text{ K}^{-1}$  [58, 59]. A temperature change of  $500^\circ\text{C}$  to the annealing temperature will only change the strain state in the films (additional to the mismatch induced strain) by less than 1%.

Depending on the mismatch, either coherent, semicoherent or even incoherent interfaces develop which in turn influence ionic conductivity positively or negatively depending on the concentration of structural defects or of tensile or compressive strain [21, 22]. In the case of YSZ/ $\text{Sc}_2\text{O}_3$ , coherent compressive strained YSZ layers are expected [28] and YSZ/ $\text{Y}_2\text{O}_3$  hetero-interfaces result in coherent tensile strained YSZ layers [26].

In coherent interfaces, which form in YSZ/ $\text{Sc}_2\text{O}_3$ - or in YSZ/ $\text{Y}_2\text{O}_3$ -multilayer systems, the lattice mismatch  $f$  is fully compensated by elastic strain. In our model systems, the elastic properties of YSZ and  $\text{Re}_2\text{O}_3$  are assumed to be similar, and thus, the strain  $\varepsilon_0$  in the individual YSZ- and in

the individual  $\text{Re}_2\text{O}_3$ -layers are equal but off opposite sign and about half of the mismatch  $f$ :

$$\varepsilon_0 \approx \frac{1}{2}f, \quad \text{with} \quad f = \frac{d_{\text{YSZ}} - d_{\text{Insulator}}}{d_{\text{YSZ}}}. \quad (4)$$

Based on these considerations,  $D_{\text{int}}$  and  $D_{\text{vol}}$  can be calculated from  $D_{\text{tot}}$ , when the extension of the strained region  $\delta$  is estimated. More details are described in former publications on conduction in the multilayer systems YSZ/ $\text{Y}_2\text{O}_3$ , YSZ/ $\text{Lu}_2\text{O}_3$  and YSZ/ $\text{Sc}_2\text{O}_3$  [21, 22, 26, 28, 29].

In these studies the ionic mobility was probed by conductivity measurements in dependence of the heterophase-boundary density, i.e. more specifically by impedance spectroscopy and the films were contacted on both sides which were uncovered by mechanical polishing. As expected from equation (1) the total ionic conductivity is increased in the case of tensile strain (YSZ/ $\text{Y}_2\text{O}_3$ ,  $f_{\text{YSZ}} = +3.04\%$ ) and decreased in case of compressive strain (YSZ/ $\text{Sc}_2\text{O}_3$ ,  $f_{\text{YSZ}} = -4.37\%$ ). No clear trend could be found in the case of the YSZ/ $\text{Lu}_2\text{O}_3$  multilayer system with only small (tensile) strain due to a mismatch  $f_{\text{YSZ}}$  of only +1.02%.

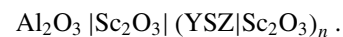
It should be noted that our theoretical model is a necessary simplification of the complex microstructure of heterophase multilayers. As discussed above, some of the misfit strain can be released by the columnar microstructure and the grain boundaries. This will lead to a smaller effect at the heterophase boundary, but can add effects at the grain boundaries.

### 3. Experimental

#### 3.1. Thin film deposition by pulsed laser deposition

All multilayer samples were prepared by PLD. Polished single-crystalline  $\text{Al}_2\text{O}_3$  (sapphire) with a (0001) surface orientation purchased from CrysTec GmbH was used as substrate material. The polycrystalline targets of YSZ ( $\text{ZrO}_2 + 9.5 \text{ mol\% Y}_2\text{O}_3$ ) were supplied by HTM Reetz GmbH, and the  $\text{Sc}_2\text{O}_3$  targets were prepared by ball milling, pressing and sintering for 48h at  $1400^\circ\text{C}$  in air, of  $\text{Sc}_2\text{O}_3$  powder (99.99%) delivered from Chempur Feinchemikalien und Forschungsbedarf GmbH.

During the ablation, the background pressure of oxygen inside the PLD chamber was set to 0.06 mbar while the temperature of the substrate was kept at  $800^\circ\text{C}$  (1073 K). For the deposition of all multilayer systems, an excimer laser (Lambda-PhysikComPEX 201, KrF) at a wavelength of  $\lambda = 248 \text{ nm}$ , a pulse energy of 150 mJ and a repetition rate of 10 Hz was used. After deposition, the multilayer samples were annealed at  $800^\circ\text{C}$  (1073 K) for 48h in air. The first and the last layer was always  $\text{Sc}_2\text{O}_3$  and this resulted in the following general multilayer structure:



A survey over all prepared samples is listed in table 2.

### 3.2. Sample preparation for diffusion experiments

For precise geometrical boundary conditions of the  $^{18}\text{O}$ -tracer-diffusion experiments the as-deposited multilayer samples had to be cut in a well defined way, to ensure that  $^{18}\text{O}_2$  can penetrate parallel to the individual layers into the sample. Therefore a slope cut was performed by the ion beam milling technique with an accelerating voltage of 7 kV, an emission current of 3.5 mA and an angle of  $90^\circ$  (Leica Micro-systems/BALTec RES 101).

As the large area multilayer samples—prepared by PLD—often showed small pin holes perpendicular to the individual layers, we had to use a metal capping layer to exclude gas permeation perpendicular to the layers. All samples were covered with a gold capping layer by thermally evaporation at 7 kV and an emission current of 3.5 A (Sputter-Coater, Tectra). With these capped and precisely ion-cut samples we were able to obtain well reproduced  $^{18}\text{O}$ -diffusion profiles (for a graphical illustration, see figure 2(a)). The  $^{18}\text{O}$ -tracer exchange experiments were performed in a special oven. The chamber was heat-treated up to  $70^\circ\text{C}$  (343 K) and simultaneously evacuated to  $1 \times 10^{-9}$  mbar before the exchange experiment to ensure absence of water, which may affect the diffusion- and the surface exchange coefficient [53], before every experiment.

### 3.3. Microstructural characterization by XRD and HR-SEM

All samples were characterized by x-ray diffraction (XRD) (Siemens Kristalloflex D500, Bragg Brentano, Cu-K $\alpha$  radiation) to determine the crystallinity, orientation and texture of the multilayer structures. The measurements were taken from  $2\theta = 20^\circ$  to  $70^\circ$  with the range between  $41.5^\circ$  and  $42.5^\circ$  omitted in order to exclude the intense (0006)  $\text{Al}_2\text{O}_3$  sapphire substrate reflection.

To evaluate the thickness of all individual layers we used high-resolution scanning electron microscopy (HR-SEM, MERLIN, Zeiss NTS). All samples were cross-sectioned and polished in two stages. First they were mechanically polished with colloidal  $\text{SiO}_2$  down to  $0.01 \mu\text{m}$  and the final polish was completed by means of an  $\text{Ar}^+$ -ion polishing/milling system with an accelerating voltage of 4 kV, an emission current of 2.8 mA and an angle of  $90^\circ$  (Leica Microsystems/BALTec RES 101). To visualize the sample width and structure of the generated slope, all samples were also investigated by HR-SEM without these polishing steps at a  $60^\circ$  angle.

### 3.4. $^{18}\text{O}$ exchange experiment

The oxygen tracer diffusion coefficient was determined from the isotope exchange depth profile by using time of flight secondary ion mass spectrometry (ToF-SIMS). ToF-SIMS software SurfaceLab V6 (IonTOF, Münster, Germany) was used to analyze all spectra and images. By employing a surface profilometer (Alpha-Step IQ Profiler, KLA-Tencor) all the individual layer thicknesses could be estimated.

The samples were heated up to  $550^\circ\text{C}$  and equilibrated in research grade dry  $^{16}\text{O}_2$  (99.999%) at a nominal pressure

of 1.5 mbar for a duration of one order of magnitude longer than the  $^{18}\text{O}_2$  tracer annealing time to ensure that initial equilibrium was achieved. Then the atmosphere was changed to 1.5 mbar  $^{18}\text{O}_2$  (Linde, 99.9%  $^{18}\text{O}_2$ ) at the same temperature and kept static for 1h. After isotopic exchange, the samples were quenched by rolling the sample holder out of the furnace. The  $^{18}\text{O}_2$  annealing time and temperature were chosen in order to ensure optimal diffusion lengths within the range of  $40\text{--}80 \mu\text{m}$ , which then offers optimal lateral resolution of the SIMS line scan.

After  $^{18}\text{O}$  isotope exchange, the gold capping layer near the edge was removed by ion beam milling with an accelerating voltage and an emission current of 3.8 kV and 2.1 mA at an incident angle of  $90^\circ$ , and the oxygen diffusion profiles were obtained by ToF-SIMS.

### 3.5. ToF-SIMS analysis

The profiles of the secondary ion intensities were measured as a function of depth using a 25 keV  $\text{Bi}^+$  primary beam with a diameter of  $5 \mu\text{m}$  (high lateral resolution) for analysis, and a 1 keV  $\text{Cs}^+$  primary ion beam for sputtering. Charge compensation was achieved with an electron flood gun. To avoid crater wall effects, the analyzed area of  $100 \mu\text{m}^2$  (directly on the edge) was centered on the  $250 \mu\text{m}^2$  sputter area.

To determine the isotope distribution as a function of sputter time, the intensities of secondary negative ions ( $^{16}\text{O}^-$ ), ( $^{18}\text{O}^-$ ), ( $^{16}\text{O}_2^-$ ), ( $^{18}\text{O}^{16}\text{O}^-$ ), ( $\text{YO}^-$ ), ( $\text{ZrO}^-$ ) and ( $\text{ScO}^-$ ) were recorded. For YSZ and  $\text{Sc}_2\text{O}_3$  a constant sputter rate was determined and thus the sputter time could be converted into sputter depth using the crater depth measured with the surface profilometer.

To obtain normalized  $^{18}\text{O}^-$  diffusion profiles, the signal intensity of  $^{16}\text{O}^-$  is needed, but due to the overdriven  $^{16}\text{O}^-$  signal intensities, the bimolecular method (see [35] in detail) was used to calculate the standardized isotope fraction  $C(x)$  of  $^{18}\text{O}^{16}\text{O}^-$  (instead of  $C(x)$  of  $^{18}\text{O}^-$ ) from the signal intensities of  $^{16}\text{O}_2^-$  and  $^{18}\text{O}^{16}\text{O}^-$ :

$$C(x) = \frac{I(x, ^{18}\text{O}^{16}\text{O})}{I(x, ^{18}\text{O}^{16}\text{O}) + 2I(x, ^{16}\text{O}_2)}. \quad (5)$$

$C(x)$  represents the standardized isotope fraction of  $^{18}\text{O}^{16}\text{O}^-$ , and  $(x, ^{18}\text{O}^{16}\text{O})$  and  $(x, ^{16}\text{O}_2)$  are the local intensities obtained from the SIMS measurements. The factor of 2 arises due to the possibilities of the formation of the individual bimolecular species. There are two possibilities to create  $^{18}\text{O}^{16}\text{O}^-$  and only one for  $^{16}\text{O}^{16}\text{O}^-$  (see [54] in detail). In [35], we neglected the factor of 2. This caused a small error in  $D_{\text{tot}}$  of less than 5%. Taking the factor of 2 properly into account, more precise results can be obtained.

In order to calculate the mean tracer diffusion coefficient  $D_{\text{tot}}$ , the calculated normalized isotopic fractions  $C'(x)$  of  $^{18}\text{O}^{16}\text{O}^-$  (written as  $^{18}\text{OO}^-$  in short in the following) were then fitted as functions of depth  $x$  to the solution of the diffusion equation for semi-infinite media derived by Crank [48].

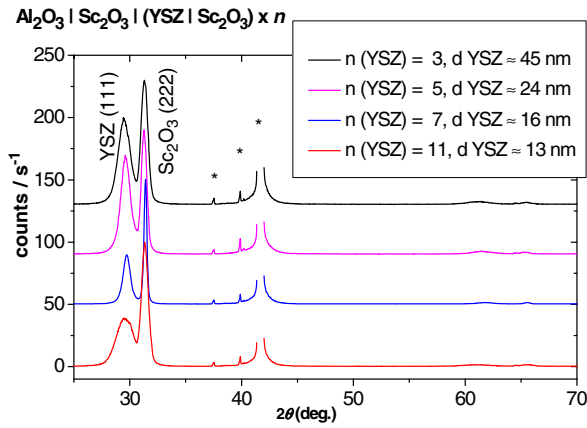


**Figure 4.** XRD patterns of the YSZ/ $\text{Y}_2\text{O}_3$  multilayer samples (normalized with respect to the (222)  $\text{Sc}_2\text{O}_3$  reflections). Reflections from the substrate are labeled with a “\*”.  $d$  ( $\text{Sc}_2\text{O}_3$ ) invariably approximately 40 nm.

$$C'(x) = \frac{C(x) - C_{\text{bg}}}{C_{\text{g}} - C_{\text{gb}}} = \text{erfc}\left(\frac{x}{2\sqrt{D_{\text{tot}}t}}\right) - \exp(hx + h^2 D_{\text{tot}}t) \text{erfc}\left(\frac{x}{2\sqrt{D_{\text{tot}}t}} + h\sqrt{D_{\text{tot}}t}\right)$$

with  $h = \frac{k}{D_{\text{tot}}}$ . (6)

$C'(x)$  represents the standardized isotope fraction of  $^{18}\text{O}$  as already described in (5),  $C_{\text{bg}}$  is the natural background isotope fraction of  $^{18}\text{O}$  in the sample at great distance from the slope cut,  $C_{\text{g}}$  is the isotope fraction of  $^{18}\text{O}$  in the gas phase and  $D_{\text{tot}}$  is the mean oxygen tracer diffusion coefficient. The parameter  $h$  combines the tracer diffusion coefficient  $D_{\text{tot}}$  and the surface exchange coefficient  $k$ . Nonlinear least squares regression on the basis of (6) was used to obtain values for  $D_{\text{tot}}$ .

## 4. Results

### 4.1. Microstructural characterization by XRD

The high signal-to-noise ratios in the XRD patterns indicate that all samples prepared by PLD were fully crystalline. Furthermore we found strongly textured multilayers on (0001)  $\text{Al}_2\text{O}_3$ -substrates with a distinctive axial orientation relationship between YSZ and  $\text{Sc}_2\text{O}_3$  as visible from the dominating intensities of (111) YSZ and (222)  $\text{Sc}_2\text{O}_3$ . According to these results, the preferred axial orientation is thus:

$$(0001) \text{Al}_2\text{O}_3 \parallel (222) \text{Sc}_2\text{O}_3 \parallel [(111) \text{YSZ} \parallel (222) \text{Sc}_2\text{O}_3]_n.$$

In figure 4, the normalized XRD patterns of all multilayer systems are given. The (222)  $\text{Sc}_2\text{O}_3$  signal could always be detected with the same signal intensity due to the constant layer thickness independent of the YSZ thickness whereas the signal intensity of the (111) YSZ reflection diminishes with decreasing layer thickness down to approximately 13 nm where it almost disappears and transforms into a shoulder of the (222)  $\text{Sc}_2\text{O}_3$  signal.

**Table 1.** Structural data for YSZ (9.5 mol%  $\text{Y}_2\text{O}_3$ ),  $\text{Sc}_2\text{O}_3$  and  $\text{Al}_2\text{O}_3$ .

Material	Structure	Space group	Lattice parameter / (Å)
YSZ	$\text{CaF}_2$	$Fm\bar{3}m$	$a = 5.143$ [45]
$\text{Sc}_2\text{O}_3$	$\alpha\text{-Mn}_2\text{O}_3$	$Ia\bar{3}$	$a = 9.846$ [46]
$\text{Al}_2\text{O}_3$	$\alpha\text{-Al}_2\text{O}_3$	$R\bar{3}c$	$a = 4.754$ $c = 12.990$ [47]

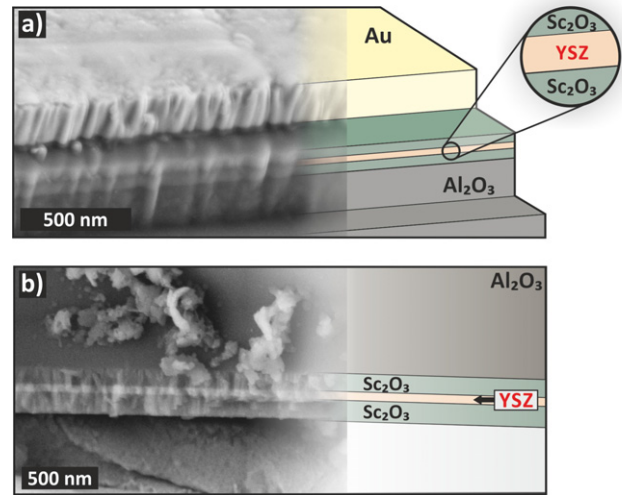


**Figure 5.** HR-SEM images of slope cut samples (by using an ion beam milling technique) at an incident angle of  $60^\circ$  (a), and cross-sectioned and subsequently polished samples (b).

**Table 2.** Overview of all investigated multilayer samples  $\text{Al}_2\text{O}_3 \parallel [\text{Sc}_2\text{O}_3 \parallel (\text{YSZ} \parallel \text{Sc}_2\text{O}_3)]_n$ . The layer thickness was determined by HR-SEM and ToF-SIMS depth profiling in combination with profilometry. The thickness of the  $\text{Sc}_2\text{O}_3$  layers in all samples was approximately 40 nm. The lattice constants were measured by XRD. # No  $\text{Sc}_2\text{O}_3$  layers.

Sample	n	$a_{\text{YSZ}}(\text{Å})$	$a_{\text{Sc}_2\text{O}_3}(\text{Å})$	$d_{\text{YSZ}}/(\text{nm})$	$D_{\text{tot}}^*(\text{cm}^2 \text{s}^{-1})$
P41	1	5.20	10.24	$45 \pm 5$	$6.7 \pm 0.4$
P45	2	5.22	10.28	$24 \pm 3$	$5.0 \pm 0.4$
P48	3	5.25	10.27	$16 \pm 2$	$3.2 \pm 0.4$
P51	5	5.25	10.26	$13 \pm 1$	$1.9 \pm 0.3$
P1	1#	5.23		$1000 \pm 50$	$8.0 \pm 0.4$

The average lattice constants  $a_{\text{YSZ}}$  and  $a_{\text{Sc}_2\text{O}_3}$  differ slightly by 1.8%, respectively 0.4%, from literature reference data [45, 46] (in detail see table 1).

### 4.2. Microstructural characterization by HR-SEM

Cross-sectioned samples were analyzed by HR-SEM to determine the layer thicknesses of all individual layers, and one example is shown in figure 5(b).

Well-ordered layers with sharp interfaces are found and we were able to determine the individual layer thicknesses. Table 2 presents the results.

In addition, to display the generated slope created by ion beam milling, all fully prepared multilayer systems without these polishing steps were investigated by HR-SEM with an angle of  $60^\circ$ , and one example is illustrated in figure 5(a).

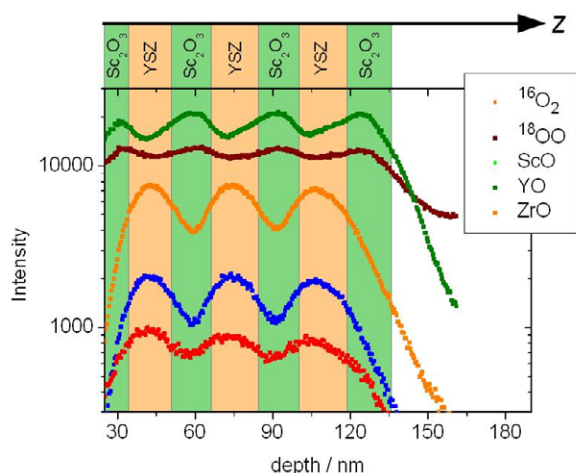


**Figure 6.** ToF-SIMS depth profile of an YSZ/Sc<sub>2</sub>O<sub>3</sub> multilayer sample in the *z*-direction with three YSZ and four Sc<sub>2</sub>O<sub>3</sub> layers.

Although it was not possible to determine the individual layer thicknesses from this perspective, at least the individual layers were visible due to the smoothness of the well laid open edge, generated by ion beam milling.

#### 4.3. SIMS Results

In figure 6, an example of a measured depth profile (primary data) is given. All individual negative ion intensities over the whole *x*-, *y*-area were summarized as a function of the depth along the *z*-axis (orthonormal to the layers, see figure 2(a)). Owing to the special arrangement of the multilayer systems during SIMS bombardment (multilayers and therefore the diffusion direction were perpendicular to the primary SIMS beam) a depth profile cannot facilitate <sup>18</sup>OO<sup>-</sup> diffusion profiles along the *x*-axis. However, this method allows the determination of the individual layer thicknesses and comparison with HR-SEM results. The microstructure of the multilayer system can be visualized with this depth profile when considering the spatial profiles of the ZrO<sup>-</sup> (orange), YO<sup>-</sup> (blue) (together the YSZ layers) and ScO<sup>-</sup> ions (green). Every maximum illustrates an individual layer and the widths of these maxima present the layer thicknesses. Unambiguously, the intensities of ZrO<sup>-</sup> and YO<sup>-</sup> ions run parallel, and the intensity of the YO<sup>-</sup> ion is always approximately 20% of the ZrO<sup>-</sup> intensity, which reflects the composition of YSZ with 10 mol% Y<sub>2</sub>O<sub>3</sub>. The spatial profile of Sc<sub>2</sub>O<sub>3</sub> is, as expected, nearly mirror-inverted, reflecting alternating Sc<sub>2</sub>O<sub>3</sub> and YSZ layers. The layer thicknesses obtained by SIMS depth profiling show good agreement with the results of HR-SEM.

The spatial intensity profiles of <sup>16</sup>O<sub>2</sub><sup>-</sup> ions (brown) were shifted to about one order of magnitude higher values compared to those of <sup>18</sup>OO<sup>-</sup> (red), but interestingly they are almost perfectly anti-parallel suggesting that <sup>16</sup>O<sub>2</sub><sup>-</sup> was substituted considerably by <sup>18</sup>OO<sup>-</sup>. The spatial profiles of the <sup>18</sup>OO<sup>-</sup> signal intensity were always nearly parallel to those of ZrO<sup>-</sup> and YO<sup>-</sup> (shifted in the majority of cases to some orders of magnitude smaller values). Hence <sup>18</sup>O<sup>-</sup> only penetrates into the individual YSZ layers and therefore

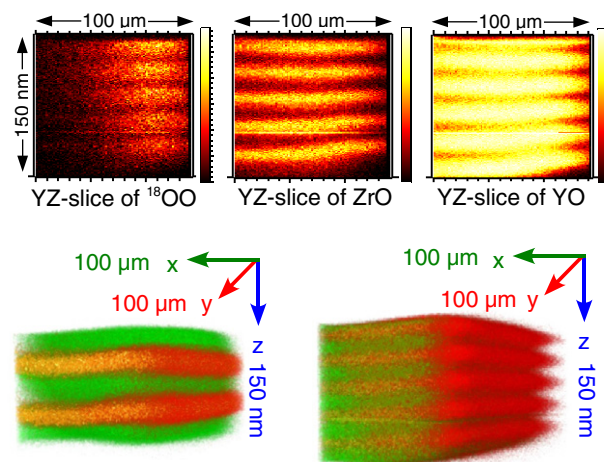


**Figure 7.** 2D and 3D elemental mapping pictures of two samples with different numbers of YSZ layers and thicknesses. The *x*- and *y*-axis were 100 μm and *z*-axis 100 nm. In the two-dimensional SIMS images, bright colors represent high concentrations of the observed element and dark colors represent low concentrations. In the three-dimensional SIMS images, Sc<sub>2</sub>O<sub>3</sub> is green, YSZ yellow and <sup>18</sup>OO red.

maxima of <sup>18</sup>OO<sup>-</sup> signal intensities were expected in YSZ layers, respectively high ZrO<sup>-</sup> and YO<sup>-</sup> signal intensities, and minima are expected in Sc<sub>2</sub>O<sub>3</sub>-layers, respectively high ScO<sup>-</sup> signal intensities. Furthermore, a penetration of <sup>18</sup>O<sup>-</sup> perpendicular to the individual layers from the top surface of the multilayer system could be excluded due to the quasi constant values of the maxima and minima of the <sup>18</sup>OO<sup>-</sup> signal intensities. Thus, the profile in figure 6 proves that the multilayers used indeed offered a perfect two-dimensional sample geometry.

To visualize the penetration of <sup>18</sup>O<sup>-</sup> into the individual YSZ layers, starting from the generated edge, and thereby to obtain diffusion profiles, two- and three-dimensional elemental maps (secondary data) were generated from the primary data.

Figure 7 illustrates the two- and the three-dimensional elemental mapping of two exemplary samples. In both samples the individual layers can all be identified. It should be noted that the *x*-, *y*-area is 100 μm<sup>2</sup> big whereas the *z*-axis corresponds only to 100 nm depth, which means that we were able to visualize individual layers with a thickness down to approximately 13 nm in 3D mode even if the length and width of the film is 10<sup>4</sup> times larger than the thickness. This result is an excellent proof for the high quality of the multilayer samples. The pictures show clearly that <sup>18</sup>O<sup>-</sup> only penetrates into the individual YSZ layers starting from the generated edge. A slightly stronger penetration in the upper layers suggests a marginal penetration of <sup>18</sup>O<sup>-</sup> perpendicular to the multilayer system from the top surface.

Based on these two- and three-dimensional elemental mappings, we evaluated <sup>18</sup>OO<sup>-</sup> line scans in the direction of the *x*-axis starting from the slope cut as shown in figure 8. As seen in figure 8, we find excellent agreement between the experimentally obtained depth profiles (black dots) and the non-linear fit (red line) of equation (6), resulting



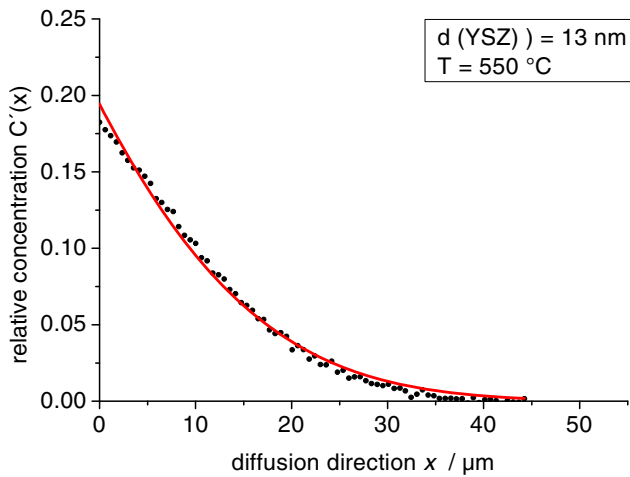


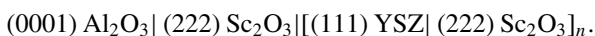
**Figure 8.** Diffusion profiles along the  $x$ -axis (parallel to the individual layers) of sample with  $d(\text{YSZ}) = 13 \text{ nm}$ . Note that each data point corresponds to the integrated  $^{18}\text{OO}^-$  concentration in a  $y$ - $z$  area at a given  $x$ . The solid red line represents the fit.

in well reproducible data for  $D_{\text{tot}}$ . Different samples of each multilayer with defined thicknesses were investigated several times and the obtained diffusion coefficients  $D_{\text{tot}}$  (arithmetic averages over these values) are summarized in table 2. These results show that the mean tracer diffusion coefficient  $D_{\text{tot}}$  decreases by a factor of 0.2 when decreasing the layer thickness of the individual YSZ layers from 45 nm down to 13 nm (respectively with an increasing density of YSZ/ $\text{Sc}_2\text{O}_3$  interfaces). The error bars were calculated as standard deviation using all the individually obtained diffusion coefficients and the arithmetic averages.

## 5. Discussion

### 5.1. Microstructural characterization by XRD

The XRD measurements show that the multilayer samples prepared in this study are strongly textured. On (0001)  $\text{Al}_2\text{O}_3$  the preferred orientation is



This agrees well with the findings of Schichtel *et al* [28]. The trifold symmetry of the [111] axis of the crystallites in the first  $\text{Sc}_2\text{O}_3$  layer corresponds to the likewise trifold symmetry of the (0001)  $\text{Al}_2\text{O}_3$  substrate surface. The observed orientation might correspond to an energy minimum. For a 4:3 commensurability between close-packed anion planes in the  $\text{Al}_2\text{O}_3$  and close-packed cation planes in the  $\text{Sc}_2\text{O}_3$  a mismatch of -4.28% is calculated. This has been proven by transmission electron microscopy (TEM) investigations; see Schichtel *et al* [28].

The crystal structures of YSZ (cubic, fluorite type) and  $\text{Sc}_2\text{O}_3$  (cubic, bixbyite type) are closely related. For the observed orientation a very good 1:1 match between the closed-packed cation planes results, which leads to well-ordered interfaces. In the case of film crystallites with constrained size ( $< 100 \text{ nm}$  diameter) strained coherent

interfaces can be found, as investigated and described in detail in the preceding article [21, 28]. The number of misfit dislocations is negligible. For YSZ and  $\text{Sc}_2\text{O}_3$  layers with given orientation a misfit of 4.46% is calculated (see table 1 for lattice parameters).

### 5.2. Transport properties from $^{18}\text{O}$ tracer measurements

The bulk diffusion coefficient  $D_{\text{vol}}$  (bulk phase) for the single 1000 nm thick YSZ thin film is in good accordance with tracer diffusion coefficient data on poly- and single-crystalline YSZ samples reported in the literature [33, 34].

The results of the tracer diffusion experiments can be compared with the results from oxygen ion conductivity measurements in YSZ/ $\text{Sc}_2\text{O}_3$  multilayers [28]. The ratio  $D_{\text{tot}}/D_{\text{vol}}$  between the mean oxygen ion diffusion coefficient of the multilayers and the value for the YSZ bulk phase are directly related to the ratio  $\sigma_{\text{tot}}/\sigma_{\text{vol}}$  of the mean oxygen ion conductivity and the bulk conductivity. Using the Nernst–Einstein equation it follows:

$$\frac{D_{\text{tot}}}{D_{\text{vol}}} = \frac{\sigma_{\text{int}} c_{\text{vol}}}{\sigma_{\text{vol}} c_{\text{int}}}. \quad (7)$$

If the concentration  $c_{\text{int}}$  of oxygen ions in the strained interface region is equal to the concentration  $c_{\text{vol}}$  in the unstrained bulk phase, the ratio  $D_{\text{tot}}/D_{\text{vol}}$  should be identical to  $\sigma_{\text{tot}}/\sigma_{\text{vol}}$  for identical samples. We can safely assume that the concentrations of oxygen in bulk and interface regions are virtually equal, as large differences would either require severe segregation of yttria or extremely strong reduction of YSZ. We have evidence neither for segregation nor reduction, and therefore we assume that the equality between the ratio of the diffusion coefficients on the one hand and the ratio of the conductivities on the other hand holds.

If we also assume that the diffusion mechanisms in the bulk and the interface region are similar (vacancy-mediated diffusion), the ratio  $D_{\text{tot}}^*/D_{\text{vol}}^*$  between the values of the tracer diffusion coefficient for a multilayer and the bulk value should be identical to the ratio  $D_{\text{tot}}/D_{\text{vol}}$  of the self diffusion coefficients in equation (7):

$$\frac{D_{\text{tot}}^*}{D_{\text{vol}}^*} = \frac{D_{\text{tot}}}{D_{\text{vol}}}. \quad (8)$$

This is valid as long as the correlation factors for the vacancy-based diffusion in the bulk and the interface regions are identical. Thus, the measured ratios  $D_{\text{tot}}^*/D_{\text{vol}}^*$  of the tracer diffusion coefficients can be directly compared to the ratios  $\sigma_{\text{tot}}/\sigma_{\text{vol}}$  from preceding conductivity studies [28]. In figure 9 the ratios  $D_{\text{tot}}/D_{\text{vol}}$  from this study (values from table 1) and the ratio  $\sigma_{\text{tot}}/\sigma_{\text{vol}}$  from a former conductivity study of YSZ/ $\text{Sc}_2\text{O}_3$  multilayers are plotted versus the reciprocal thicknesses  $1/d$  of the YSZ layers [28]. The single 1000 nm-thick YSZ thin film is taken as reference for the bulk value  $D_{\text{vol}}$ . In the same graph, values for  $\sigma_{\text{tot}}/\sigma_{\text{vol}}$  and  $D_{\text{tot}}/D_{\text{vol}}$  of YSZ/ $\text{Y}_2\text{O}_3$  multilayers from former studies are also plotted [26, 35]. The temperature ranges used in the different studies are comparable, i.e. conductivity/diffusion

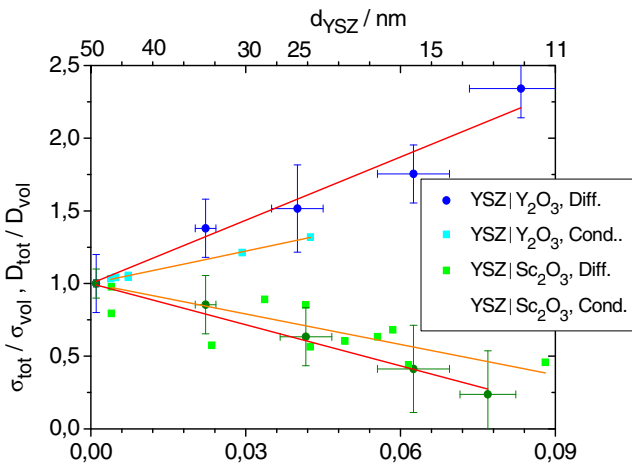


**Figure 9.** Dependency of the ratio  $D_{\text{tot}}/D_{\text{vol}}$  between the total oxygen ion diffusion coefficient and the bulk value on the reciprocal layer thickness  $1/d$  (squares). Analogous data  $D_{\text{tot}}/D_{\text{vol}}$  and  $\sigma_{\text{tot}}/\sigma_{\text{vol}}$  from former tracer diffusion and conductivity studies are plotted in the same graph (bright circles, Schichtel [13] and Peters [11], and blue dots Aydin [35]).

**Table 3.** Slopes of  $D_{\text{tot}}/D_{\text{vol}}$  respectively  $\sigma_{\text{tot}}/\sigma_{\text{vol}}$  plotted versus  $1/d$  for different multilayer systems and research methods.

Multilayer	Study	Slope(nm <sup>-1</sup> )
YSZ Sc <sub>2</sub> O <sub>3</sub>	Tracer diffusion, $D_{\text{tot}}/D_{\text{vol}}$	-9.5 ± 0.5
YSZ Sc <sub>2</sub> O <sub>3</sub>	AC-impedance, $\sigma_{\text{tot}}/\sigma_{\text{vol}}$	-7.0 ± 0.8
YSZ Y <sub>2</sub> O <sub>3</sub>	Tracer diffusion, $D_{\text{tot}}/D_{\text{vol}}$	14.5 ± 0.9
YSZ Y <sub>2</sub> O <sub>3</sub>	ac-impedance, $\sigma_{\text{tot}}/\sigma_{\text{vol}}$	7.4 ± 0.1

were studied in YSZ|Sc<sub>2</sub>O<sub>3</sub> at 560 °C/550 °C and in YSZ|Y<sub>2</sub>O<sub>3</sub> at 560 °C/520 °C. The errors given in figure 9 for the diffusion data are calculated by using the error margins specified in table 2.

In view of the difficult experiments with complex samples, the results of the tracer diffusion experiments are in excellent agreement with the former conductivity measurements. This is the case for the YSZ|Sc<sub>2</sub>O<sub>3</sub> multilayers as well as for the YSZ|Y<sub>2</sub>O<sub>3</sub> multilayers from a former study. For YSZ|Sc<sub>2</sub>O<sub>3</sub> multilayers, the total oxygen ion diffusion coefficient  $D_{\text{tot}}/D_{\text{vol}}$ , respectively the total oxygen ion conductivity  $\sigma_{\text{tot}}/\sigma_{\text{vol}}$  relative to the bulk values, decrease with decreasing YSZ layer thickness  $d$  (increasing phase boundary density,  $\sim 1/d$ ). In the case of YSZ|Y<sub>2</sub>O<sub>3</sub> multilayers,  $D_{\text{tot}}/D_{\text{vol}}$  and  $\sigma_{\text{tot}}/\sigma_{\text{vol}}$ , increase with decreasing YSZ layer thickness  $d$ .

As expected from equation (2), a linear relationship between  $D_{\text{tot}}/D_{\text{vol}}$ , respectively  $\sigma_{\text{tot}}/\sigma_{\text{vol}}$  and  $1/d$ , is found, as long as the thickness  $d$  of the conducting layers is large compared to the extent  $\delta$  of the strained interface region with modified transport properties. Consequently, the strained interface region is thinner than the thinnest YSZ layers ( $d_{\text{YSZ}} = 13$  nm). Thus, it will probably not exceed 5 nm. Using linear regression the slopes can be calculated. The data for a fixed intercept with the ordinate at 1 are summarized in table 3.

The slope in the case of the conductivity data does not exceed the values of the diffusion data. This implies

that in these multilayers the measured ‘thin film effect’ on the oxygen ion conduction  $\sigma_{\text{tot}}/\sigma_{\text{vol}}$  does not include any significant electronic transport. Thus, the change of the mean transport properties in these multilayers can be attributed only to a modified oxygen ion transport along the (compressively or tensile strained) interfaces.

However, despite precise results from these tracer diffusion experiments, we were not able to determine an activation volume because our experimental temperature range is very small. The main challenge for future experiments is to prepare even better capping layers. The gold capping layer was only gastight for temperatures below 580 °C. But at these lower temperatures a reliable diffusion profile for <sup>18</sup>O cannot be obtained in our multilayers due to the short diffusion length. As well described in [55], a Bi<sup>+</sup>-ion primary beam with a diameter of 5 μm requires a minimal diffusion length of about 60 μm in order to obtain  $D_{\text{tot}}$  with an average error of less than 10%. If this cannot be achieved, a systematic deviation of the fit from the measured data points can be observed with an underestimation at the beginning and an overestimation at the end of the diffusion profiles.

However, even if our diffusion lengths are only about 40 μm, the deviation of the fit from the data points is very small, and thus, the results presented here are sufficiently precise.

### 5.3. Application of a strain-based model

As already discussed in some detail in the section on the microstructural characterization, a significant part of the lattice misfit is released by elastic strain, indicated by the coherent structure of the heterophase boundaries between the adjacent YSZ and Sc<sub>2</sub>O<sub>3</sub> crystallites. Because of the comparable elastic properties of YSZ, Y<sub>2</sub>O<sub>3</sub> and Sc<sub>2</sub>O<sub>3</sub> the elastic deformation caused by the misfit will divide up in nearly equal parts of compressive and tensile strain in the adjacent crystallites. Thus, for the YSZ layers a compressive strain  $\varepsilon_0$  of about -2.2% can be estimated in the case of YSZ/Sc<sub>2</sub>O<sub>3</sub> multilayers and a tensile strain of about 1.5% for YSZ/Y<sub>2</sub>O<sub>3</sub> multilayers.

The oxygen ion diffusion coefficient  $D_{\text{int}}/D_{\text{vol}}$  and the oxygen ion conductivity  $\sigma_{\text{int}}/\sigma_{\text{vol}}$  of a strained interface region, normalized to the bulk isotropic material can be calculated by equations (1) and (7). The activation volume of YSZ (9.5 mol% Y<sub>2</sub>O<sub>3</sub>) is reported in the literature as 2.08 cm<sup>3</sup> mol<sup>-1</sup> at a temperature of 750 °C [49]. The elastic parameters of cubic YSZ depend considerably on the crystallographic directions and temperature [50–52]. For the given temperature and the crystallographic orientation used in this and the former studies a value of 167 GPa for Young’s modulus and 0.38 for Poisson’s ratio can be estimated.

Using the available data from literature and the estimated interface strain, the values  $D_{\text{int}}/D_{\text{vol}}$  and  $\sigma_{\text{int}}/\sigma_{\text{vol}}$  have been calculated (see table 4). These theoretical values for  $D_{\text{int}}/D_{\text{vol}}$  and  $\sigma_{\text{int}}/\sigma_{\text{vol}}$  should be considered as upper limits for  $D_{\text{tot}}/D_{\text{vol}}$  and  $\sigma_{\text{tot}}/\sigma_{\text{vol}}$  as they rely on the assumption that the misfit is exclusively released by elastic strain.

**Table 4.** Calculated values for  $D_{\text{int}}/D_{\text{vol}}$  and  $\sigma_{\text{int}}/\sigma_{\text{vol}}$ . Estimated values for the extend  $\delta$  of the strained interface region. # Thinnest layer only 25 nm thick.

Multilayer	Study	T(°C)	$D_{\text{int}}/D_{\text{vol}}$ or $\sigma_{\text{int}}/\sigma_{\text{vol}}$	$\delta$ (nm)
YSZ Sc <sub>2</sub> O <sub>3</sub>	Tracer diffusion	550	0.3	6.9
YSZ Sc <sub>2</sub> O <sub>3</sub>	AC-impedance	560	0.4	5.1
YSZ Y <sub>2</sub> O <sub>3</sub>	Tracer diffusion	520	2.3	5.3
YSZ Y <sub>2</sub> O <sub>3</sub>	AC-impedance	560	1.3#	2.7

As discussed above, part of the misfit is also released by the formation of dislocations along the columnar grain boundaries, so that the measured effect has to be smaller than the theoretical limit.

The smallest, respectively the highest values measured for  $D_{\text{tot}}/D_{\text{vol}}$  in YSZ/Sc<sub>2</sub>O<sub>3</sub> and YSZ/Y<sub>2</sub>O<sub>3</sub> multilayers are close to the calculated values. Thus, the mismatch induced strain  $\epsilon_0$  in the YSZ layer explains well the observed effect.

Using the calculated values for  $D_{\text{int}}/D_{\text{vol}}$  and  $\sigma_{\text{int}}/\sigma_{\text{vol}}$  and the slopes of the diffusion and conductivity data versus  $1/d$  listed in table 3, the extension  $\delta$  of the strained interface region can also be estimated. The calculated values are equal to, respectively appreciably smaller than the half of the thickness of the thinnest investigated YSZ layers, i.e. less than 5 nm.

## 6. Conclusions

When comparing these results with previous tracer diffusion experiments of Aydin *et al* [35] with YSZ/Y<sub>2</sub>O<sub>3</sub> multilayer systems (in this case tensile strain is exerted on YSZ), tailoring of the diffusion coefficient in dependence of the value and strain type (tensile or compressive) is possible. Furthermore, previous conductivity experiments of Korte *et al* [26] and Schichtel *et al* [28] could be confirmed by tracer diffusion experiments with the Nernst–Einstein equation, and this implies that an electronic contribution to the measured total conductivity can be excluded. However, even if it is possible to increase or decrease the ionic conductivity by a factor of about 2 when decreasing the layer thickness down to 15 nm in a tensile or compressive strained coherent interface, or in case of incoherent interfaces increasing the ionic conductivity by 2 orders of magnitude [29], larger strain effects as reported in [18] still have to be verified.

## Acknowledgments

We are grateful to the Federal State of Hessen for financial support. Our thanks also goes to M Rohnke for help with and introduction to the ToF-SIMS depth profiling technique, and R Dippel for help with and introduction to HR-SEM.

## References

- [1] Tuller H 2000 *Solid State Ion.* **131** 143
- [2] Indris S, Heitjans P, Roman H E and Bunde A 2000 *Phys. Rev. Lett.* **84** 2889
- [3] Guo X, Tan C and Yuan R-Z 1995 *J. Eur. Ceram. Soc.* **15** 25
- [4] Heitjans P and Indris S 2003 *J. Phys.: Condens. Matter* **15** 1257
- [5] Wagner J B and Jiang S 1995 *J. Phys. Chem. Solids* **56** 1101
- [6] Maier J 1994 *Solid State Ion.* **71** 43
- [7] Kosacki I, Rouleau C, Becher P, Bentley J and Lowndes D 2005 *Solid State Ion.* **176** 1319
- [8] Kosacki I, Suzuki T and Petrovsky V 2000 *Solid State Ion.* **136–137** 1225
- [9] Kosacki I, Rouleau C M, Becher P F, Bentley J and Lowndes D H 2004 *Electrochem. Solid State Lett.* **7** A459
- [10] Sata N, Eberman K, Eberl K and Maier J 2000 *Nature* **408** 946
- [11] Maier J 2005 *Nature Mater.* **4** 805
- [12] Kim H-R, Kim J-C, Lee K R, Ji H-I, Lee H-W, Lee J-H and Son J-W 2011 *Phys. Chem. Chem. Phys.* **13** 6133
- [13] Mohan Kant K, Esposito V and Pryds N 2012 *Appl. Phys. Lett.* **100** 033105
- [14] De Souza R A, Ramadan A and Hörner S 2012 *Energy Environ. Sci.* **5** 5445
- [15] Rupp J L 2012 *Solid State Ion.* **207** 1
- [16] Araki W and Arai Y 2011 *Solid State Ion.* **190** 75
- [17] Subramanian K R S, Sankaranarayanan and Ramanathan S 2011 *J. Chem. Phys.* **134** 064703
- [18] Garcia-Barriocanal J, Rivera-Calzada A, Varela M, Sefrioui Z, Iborra E, Leon C, Pennycook S J and Santamaría J 2009 *Science* **324** 465
- [19] Guo X 2011 *Scr. Mater.* **65** 96
- [20] Cavallaro A, Burriel M, Roqueta J, Apostolidis A, Bernardi A, Tarancón A, Srinivasan R, Cook Stuart N F, Hamish L and Kilner J A 2010 *Solid State Ion.* **181** 592
- [21] Korte C, Schichtel N, Hesse D and Janek J 2009 *Mon. Chem.* **140** 1069
- [22] Schichtel N, Korte C, Hesse D and Janek J 2009 *Phys. Chem. Chem. Phys.* **11** 3043
- [23] Dezanneau G, Hermet J and Dupé B 2011 *Int. J. Hydrog. Energy* **37** 8081
- [24] Araki W, Kuribara M and Arai Y 2011 *Solid State Ion.* **193** 5
- [25] Fabbri E, Pergolesi D and Traversa E 2010 *Sci. Technol. Adv. Mater.* **11** 054503
- [26] Korte C, Peters A, Janek J, Hesse D and Zakharov N 2008 *Phys. Chem. Chem. Phys.* **10** 4623
- [27] Gerstl M, Frömling T, Schintlmeister A, Hutter H and Fleig J 2011 *Solid State Ion.* **184** 23
- [28] Schichtel N, Korte C, Hesse D, Zakharov N, Butz B, Gerthsen D and Janek J 2010 *Phys. Chem. Chem. Phys.* **12** 14596
- [29] Peters A, Korte C, Hesse D, Zakharov N and Janek J 2007 *Solid State Ion.* **178** 67
- [30] Kushima A and Yildiz B 2010 *J. Mater. Chem.* **20** 4809
- [31] Kushima A and Yildiz B 2009 *ECS Trans.* **25** 1599
- [32] Cavallaro A, Ballesteros B, Bachelet R and Santiso J 2011 *Cryst. Eng. Commun.* **13** 1625
- [33] Manning P S, Sirman J D, Souza R A De and Kilner J A 1997 *Solid State Ion.* **100** 1
- [34] De Souza R A, Pietrowski M J, Tamburini A, Kim S, Munir Z and Martin M 2008 *Phys. Chem. Chem. Phys.* **10** 2067
- [35] Aydin H, Korte C, Rohnke M and Janek J 2013 *Phys. Chem. Chem. Phys.* **15** 1944
- [36] Azad S *et al* 2005 *Appl. Phys. Lett.* **86** 131906
- [37] Korte C 2008 *Habilitationsschrift* Justus-Liebig-University Giessen Institute of Physical Chemistry
- [38] Brossmann U, Södervall U, Würschum R and Schaefer H E 1999 *Nanostruct. Mater.* **12** 871
- [39] Chater R J, Carter S, Kilner J A and Steele B C H 1992 *Solid State Ion.* **53–56** 859
- [40] Röwer R, Knöner G, Reimann K, Schaefer H-E and Södervall U 2003 *Phys. Status Solidi (b)* **239** R1

- [41] Sirman J D, Manning P S and Kilner J A 1997 *Solid State Ion.* **93** 125
- [42] Souza R A D and Martin M 2009 *MRS Bull.* **34** 907
- [43] Weller M 2004 *Solid State Ion.* **175** 409
- [44] Pergolesi D, Fabbri E, Cook S N, Roddatis V, Traversa E and Kilner J A 2012 *ACS NANO* **6**(12) 10524–34
- [45] Yashima M, Sasaki S, Kakihana M, Yamaguchi Y, Arashi H and Yoshimura M 1994 *Acta Crystallogr. B* **50** 663
- [46] Hanic F M H 1984 *Acta Crystallogr. B* **40** 76
- [47] Ishizawa B Y N, Miyata T, Minato I, Mo F M and Iwai S 1979 *Acta Crystallogr. B* **36** 228
- [48] Crank J 1975 *The Mathematics of Diffusion* 2nd edn (Oxford: Oxford University Press) p 28
- [49] Park E T and Park J-H 1998 Invited paper submitted to *3rd Int. Meeting of Pacific Rim Ceramic Societies*
- [50] Pace N G, Saunders G A, Sümengen Z and Thorp J S 1969 *J. Mater. Sci.* **4** 1106
- [51] Kandil H M, Greiner J D and Smith J F 1984 *J. Am. Ceram. Soc.* **67** 341
- [52] Kushi T, Sato K, Unemoto A, Hashimoto S, Amezawa K and Kawada T 2011 *J. Power Sources* **196** 7989
- [53] De Souza R A and Chater R J 2005 *Solid State Ion.* **176** 1915
- [54] De Souza R A and Martin M 2008 *Phys. Chem. Chem. Phys.* **10** 2356
- [55] Kilner J A and De Souza R A 1996 *Riso Int. Symp. on Materials Science: High Temperature Electrochemistry: Ceramics and Metals*
- [56] Fleig J, Rodewald S and Maier J 2000 *Solid State Ion.* **137** 905
- [57] Harrison B 1960 *Trans. Faraday Soc.* **57** 1191
- [58] Bayer G 1973 *Proc. Br. Ceram. Soc.* **22** 129
- [59] Adams J W and Nakamura H H 1985 *J. Am. Ceram. Soc.* **68** C-228